Circular Constraint Nutation Damper

W. F. CARTWRIGHT,* E. C. MASSINGILL,† AND R. D. TRUEBLOOD‡
General Motors Corporation, Goleta, Calif.

The use of passive nutation dampers to confine the angular velocity of spinning vehicles to the axis of major moment of inertia is reviewed briefly. A physical description of the damper action is given and a simple set of approximate equations provided. Exact solutions of the equations describing the motion of the circular constraint nutation damper are compared with experimental results that verify the analysis. Expressions suitable for preliminary damper design are derived, with a short discussion of multiple dampers and fluid dampers.

Introduction

THE use of vehicle spin to achieve space-stabilized orientation of the principal axis of extra-atmospheric probes and artificial satellites is employed primarily because of the simplicity that this technique lends to vehicle control system design. In particular, for a vehicle that is permitted to spin about its *major* moment of inertia axis, a simple mechanical dissipative device may be used to eliminate any unwanted transverse angular velocities that are introduced. These devices, termed "passive nutation dampers," obviate the need for angular rate transducers, power supplies, and complicated servos.

A variety of passive nutation damper designs now are extant.[1, 2] This paper presents the approximate equations that govern the operation of one such damper—the circular constraint nutation damper—and offers insight into the design stratagems required to optimize their overall performance.

Circular Constraint Damper

To be effective, a damper must perform three functions: it readily must extract angular momentum from the transverse rotation of the disk; it must transfer a large fraction of the transverse rotational energy into spin energy, thus spinning up the disk; and it must dissipate some energy to heat.

A circular constraint damper possesses features that are particularly appropriate to all three functions the damper must perform. A variety of circular constraint damper designs are possible, the earliest being the Naval Ordnance Test Station Mercury Damper. The fundamental features of any of these designs can be explained most easily by reference to the ball and rod version (Fig. 1).

The damper consists of a mass m placed on one end of a light rod of length ρ. The other end of the rod is attached to the axis of symmetry of the disk a distance h above the center of mass of the principal body. The attachment allows the rod to assume any angular position around the configuration axis of the disk. It is not necessary that the attachment maintain the rod in a plane parallel to the disk plane, but both the mechanical construction and the analysis of the damper are facilitated by specifying that the mass always be a distance h above the disk. It is particularly important to furnish a frictional restraint at the attachment point. Damping will occur for a large range of friction coefficients, but there is a value that will produce the most rapid damping.

It will be observed from Fig. 1 that the disk plus damper is not a symmetric configuration, and the principal axis of the total system does not lie along the disk configuration axis. This does not affect the damping action of the nutation damper but means only that the body, when damped, will execute a small wobble at the spin rate. This remaining spin wobble will disappear if the mass, at the end of the nutation damping action, is allowed to spread out in a ring of radius ρ, as it does with a liquid damper in a circular race.

The damper construction is completely specified by the four parameters m,ρ,h, and C_f, the coefficient of friction at the rod attachment point.

Damper Motion

The operation of the circular constraint damper is critically dependent on the difference between the spin rate of the body and the rotation rate of the transverse angular velocity vector $\boldsymbol{\Omega}_t$ around the spin axis. In the absence of damping, $\boldsymbol{\Omega}_t$ rotates about the disk symmetry axis at a rate faster than the disk spin rate. This rotation rate is known as the nutation rate (or Euler rate, in the discussion of the earth's free nutation) and is equal to $1/r$ times the spin rate, where r is the transverse to polar mass moment of inertia ratio of the disk. The transverse angular velocity component thus "sweeps" past a fixed point on the disk $(1 - r)\Omega_{spin}/2\pi r$ times/sec.

A rigorous analysis of the damper mass motion[3] shows that, in the absence of any friction at the rod attachment point, the mass has an equilibrium position that rotates in synchronism with the transverse angular velocity vector; that is, the rod spins around the disk symmetry axis faster than the disk itself spins. An intuitive argument shows physically why this represents stable damper mass motion: the damper mass, in the centrifugal force field of the instantaneous angular velocity $\boldsymbol{\Omega}$ of the disk, is flung outward, as far from $\boldsymbol{\Omega}$ as the rod constraint will permit. From Fig. 2, it is seen that this maximum outward position places the damper mass opposite the direction of the transverse angular velocity vector, and therefore the damper mass does, indeed, rotate in synchronism with the transverse angular velocity.

With friction present at the rod attachment point, the equilibrium position of the damper mass lags behind this no-friction equilibrium position. The lag angle is crucial in order for damping to ensue. This point will be discussed in detail in the following sections. As damping proceeds, the lag angle gradually increases, or, alternatively stated, the damper mass slowly slips out of synchronism with the rotation of the transverse angular velocity vector. As the lag angle increases the damping rate increases, producing a convex damping time history that is characteristic of the "nutation-synchronous" damping mode.

Unfortunately, the "nutation-synchronous" damping mode

Received by ARS September 24, 1962; revision received April 18, 1963.

* Formerly with General Motors Defense Research Laboratories. Presently with Philco Division of Ford Motor Company.

† Senior Engineering Staff, Weapons and Space Systems Laboratory, Aerospace Operations, GM Defense Research Laboratories, General Motors Corporation. Member AIAA.

‡ Head, Weapons and Space Systems Laboratory, Aerospace Operations, GM Defense Research Laboratories, General Motors Corporation.

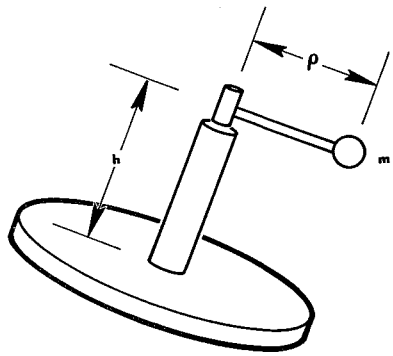

Fig. 1 Essential elements of a circular constraint damper and its attachment to a spinning vehicle

does not persist. At the instant the lag angle reaches 90° (when the damping rate is maximum), the damper mass slips *completely* out of synchronism with Ω_t and is driven toward synchronism with the spin rate of the disk. The "spin-synchronous" damping mode is characterized by a concave or exponential-like decay upon which is superimposed a convergent oscillation.

Both the nutation-synchronous and the spin-synchronous damping modes are evident in the experimental data. Figure 3 shows a typical time history of the nutation cone half angle γ for a disk equipped with a circular constraint damper. For this particular test run, the nutation-synchronous damping mode ceased, and the spin-synchronous damping mode began after the first 9 sec.

Thus the task of designing a circular constraint nutation damper becomes a twofold problem: how should the values of m,ρ,h, and C_f be selected so as to maximize the γ decay rate in the nutation-synchronous damping mode, and what must these values be in order to inhibit onset of the spin-synchronous damping mode until a very small nutation angle is reached? To answer these questions, it is necessary to employ the equations that describe the disk and damper motions.

Disk-Damper Equations

The rigorous equations of motion of the disk and damper are derived in Ref. 3. Shown in Fig. 4 is a photograph of a typical damper mounted on one of the disk-gyros used in the experimental investigation of the validity of these equations.

Figure 5 shows an experimentally determined time history of the nutation angle γ as the disk nutation is damped. The small effect of the gravitational torque exerted through the unbalanced damper mass was not subtracted from the experimental data. The time history as computed by the exact equations is shown as the solid curve. (The frictional force on the damper mass, only roughly known, was approxi-

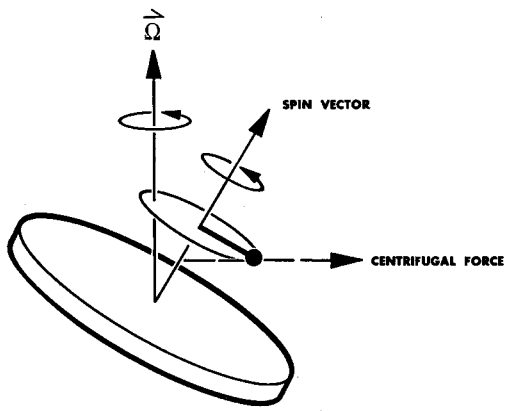

Fig. 2 Position of the damper mass for a frictionless damper

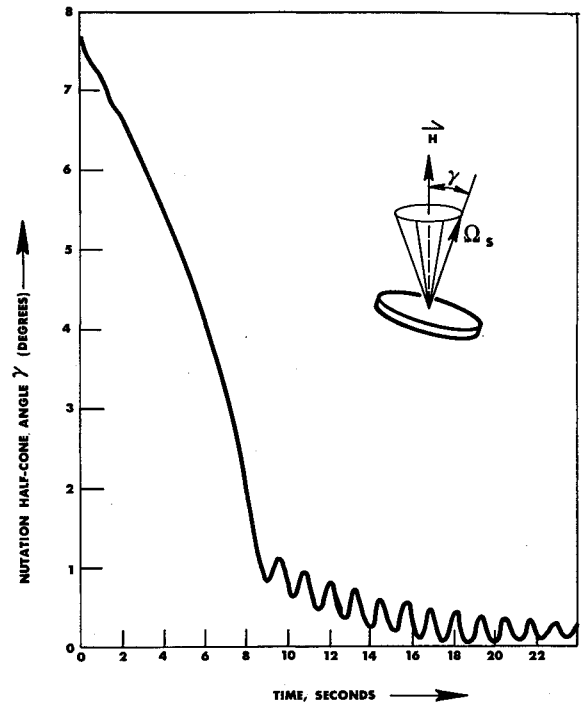

Fig. 3 Typical time history of the nutation cone angle for a vehicle equipped with a circular constraint damper

mated by a constant C_f times the relative velocity.) The agreement between experimental and simulated damping is typical and is regarded as adequate demonstration of the validity of the equations.

The exact equations are, unfortunately, so unwieldy that a physical understanding of the damper action cannot be elicited from them readily. However, by using only the principal terms of these exact equations and making use of the (good) approximation that the transverse angular velocity vector rotates precisely at the nominal nutation rate Ω_{spin}/r, a simple set of two equations is obtained (see Appendix):

$$\dot{\gamma} = \frac{m\rho h}{I_T}\left(\frac{I_P}{I_T}\Omega_s\right)\sin\alpha \tag{1}$$

$$\ddot{\alpha} + \frac{C_f}{m}\dot{\alpha} + \frac{h}{\rho}\left(\frac{I_P}{I_T}\Omega_s\right)^2\gamma\sin\alpha = -\frac{C_f}{m}\left(\frac{I_P - I_T}{I_T}\right)\Omega_s \tag{2}$$

where I_P and I_T are the polar and transverse mass moments of inertia, respectively, and α is the angle between the damper rod and the transverse angular velocity vector (Fig. 6).

It is possible, using these simplified equations, to obtain an appreciation of the damper action. From Eq. (1) it is clear what a crucial role the "lag angle" α plays in the damping. Equation (2) determines the behavior of α and is the same equation as that which governs the friction driven pendulum of Fig. 7. This pendulum is the mechanical analog of the damper mass as seen from a reference frame rotating at the nutation rate. The pendulum is of length ρ and has a bob of mass m. The forces on the pendulum bob are the gravitational force and the drag on the friction wheel. The gravitational field of the equivalent analog pendulum is characterized by a g equal to $h(\Omega_s/r)^2\gamma$. It is seen, then, that the equivalent g field decreases as the nutation angle γ decays. The pendulum bob equilibrium position is given by

$$\sin\alpha_E = -\frac{C_f}{m}\frac{\rho}{h}\left[\frac{I_P - I_T}{I_P}\right]\frac{I_T}{I_P\Omega_s}\left[\frac{1}{\gamma}\right] \tag{3}$$

This equilibrium position exists only in the fourth quadrant As γ decreases, the equilibrium position of the bob slowly moves from some small negative angle to $-\pi/2$. At this time a radical change ensues, since there exists no equilib-

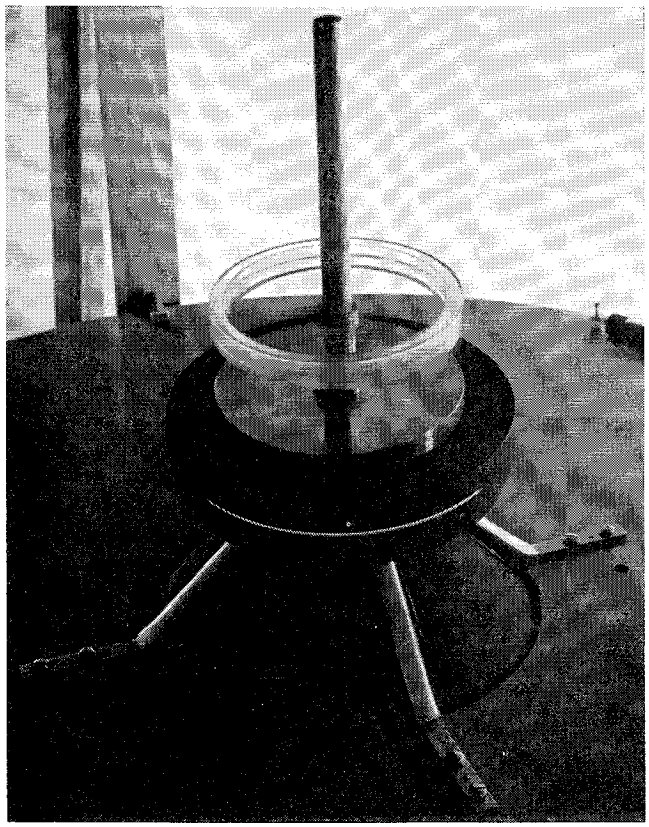

Fig. 4 Apparatus employed in damper experiments

rium value of α; the bob is dragged by the friction wheel "over the top" and continues to rotate in the clockwise direction. Thus the action of the damper can be described as follows.

In the absence of nutation, the damper mass rotates at the same speed as the friction wheel: at spin rate as seen by a fixed observer, or at the negative difference between nominal nutation and spin rate as seen by an observer viewing the mechanical analog. An external torque impulsively applied to the main body produces, suddenly, a transverse angular velocity. This Ω_t is represented in the mechanical analog by a gravitational field that suddenly is "turned on." For a sufficiently strong field (large impulse), the

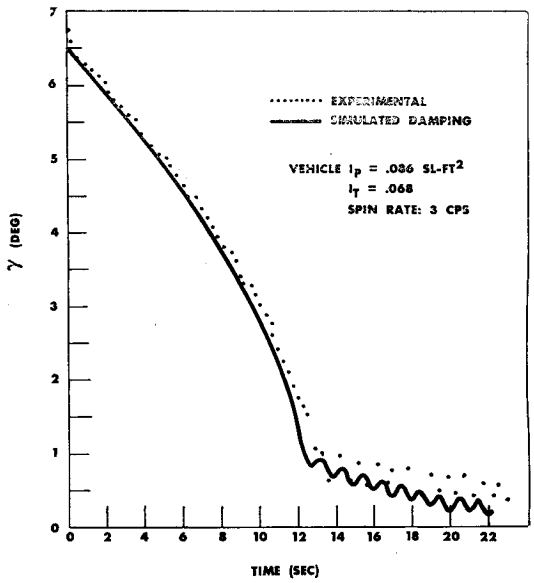

Fig. 5 Comparison of computed and experimentally determined nutation damping

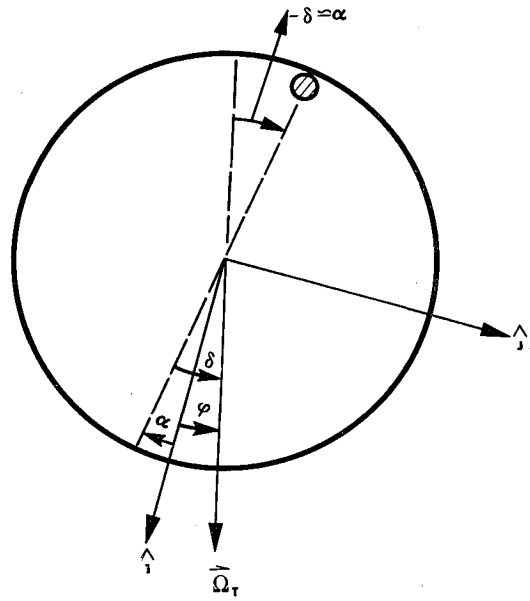

Fig. 6 Definition of variables occurring in exact and approximate equations; angles are taken positive in the counterclockwise direction

initial rotation rate and the drag of the friction wheel are unable to pull the bob "over the top." The damper mass thus performs a damped oscillation about the equilibrium position. Soon the mass assumes the equilibrium position, with the drag of the friction wheel balanced by the restoring force of gravity. The rapid nutation-synchronous damping occurs while the mass is in equilibrium.

The equilibrium direction, defined by the angle α_E, is measured in the reference frame of the mechanical analog, which is rotating at the nominal nutation rate Ω_s/r. Thus, when the damper mass has settled down to the bob equilibrium position given by Eq. (3), it is moving faster than the spinning body, just as is $\boldsymbol{\Omega}_t$, by the angular velocity difference $(1 - r)\Omega_s/r$.

As $\boldsymbol{\Omega}_t$ decays, the gravitational restoring force decreases, and the equilibrium position moves gradually to $\alpha_E = -\pi/2$. The damping rate $\dot{\gamma}$ increases as this occurs, inasmuch as it is proportional to $\sin\alpha_E$ [Eq. (1)].

When α_E passes from the fourth to the third quadrant, the bob continues "over the top," and the damper mass no longer rotates, unidirectionally, faster than the spinning body, but alternately moves faster and then slower than the spin rate. This oscillation, however, is nonlinear, the damper mass spending more time during each oscillation period moving faster than (and thus speeding up) the body than it spends moving slower (despinning the body). Thus

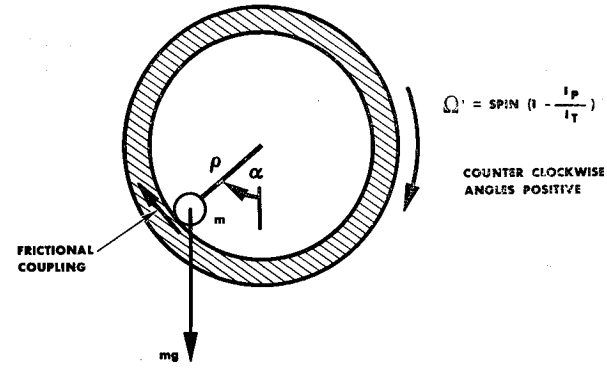

Fig. 7 Analog of the circular constraint damper; the equivalent gravitational field decreases as the nutation angle decays

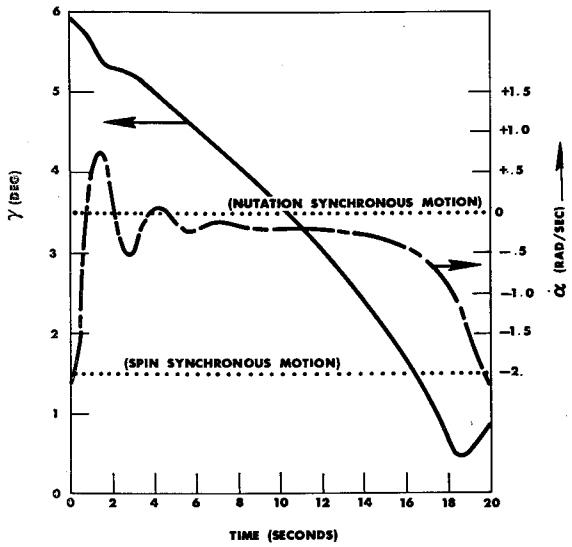

Fig. 8 Typical damper mass rotation rate during decay of the vehicle nutation angle; departure of the mass motion from exact synchronism with the nutation rate should be noted

this "spin-synchronous" mode still damps the nutation, but at a rather slow rate. In this mode, the circular constraint damper is similar in action to the "Frahm" or pendulum-type nutation dampers.

The virtue of the circular constraint damper is the complete angular freedom that the damper-body coupling allows the damper mass. By permitting the damper mass to assume a unidirectional rotation rate, the mass, driven by the nutation, can approach the nutation rate and continuously exert a spin-up torque on the body, thus producing monotonic damping.

Now proceed to estimate γ^* and t^*, the nutation cone angle and time, respectively, at the transition from nutation-synchronous to spin-synchronous damping, in terms of the parameters ρ,h,m, and C_f. These parameters then can be chosen so as to make t^* and γ^* both as small as possible.

Transition Angle and Damping Time

The nonlinear set of Eqs. (1) and (2) are not integrable as they stand, and a somewhat crude approximation must be made in order to arrive at a simple expression for γ vs time. This approximation is based on the observation that the damper mass rotates at a rate very close to the nutation rate, and thus $\dot{\alpha}$ is quite small. It must be emphasized here that, in fact, the damper mass *never* reaches exact synchronism with the nutation rate. Nevertheless, innumerable machine integrations of the exact damper equations show that for the purpose of making a crude estimate of damper performance $\dot{\alpha}$ can be neglected, and Eqs. (1) and (2) then become integrable. (Figure 8 is a typical $\dot{\alpha}$ vs time plot and shows the departure of $\dot{\alpha}$ from zero during the nutation-synchronous mode.)

With $\dot{\alpha}$ set to zero, the integrated equations lead to the following expressions:

$$\gamma^* = C_f \left(\frac{\rho}{hm}\right) \frac{1}{\Omega_s} [r(1-r)] \tag{4}$$

$$t^* = \frac{\gamma_0^2 - \gamma^{*2}}{C_f \rho^2} \left[\frac{r}{1-r}\right] \frac{I_P}{2} \tag{5}$$

where γ_0 is the initial nutation half cone angle, t^* is the transition time from nutation-synchronous to spin-synchronous damping, and γ^* is the nutation half cone angle at the time of transition.

These formulas permit preliminary performance estimates to be made of both ball and fluid circular constraint dampers. Numerical integration of the exact equations was performed for vehicles possessing moments of inertia of from 0.1 to 10 slug-ft^2 and spin rates of from $\frac{1}{6}$ to 3 cps. Equation (4) was found to overestimate γ^* by as much as a factor of 2, a consequence of assuming $\dot{\alpha}$ to be zero. Equation (5), in general, underestimates the damping time also by as much as a factor of 2.

Neither Eq. (4) nor (5) is valid when the time required for the bob to settle down to the equilibrium position is large compared with t^*, in which case the damping time can greatly exceed t^*. Reference to Eq. (2) shows that this transient damping time is approximately m/C_f. Thus m/C_f must be smaller than t^* as calculated by Eq. (5) if the latter is to be valid. Therefore, (5) is valid only if the following inequality obtains:

$$m\rho^2 \ll I_P \gamma_0^2 [r/(1-r)] \tag{6}$$

Fluid Dampers

The version of the circular constraint damper originally and most frequently used is one in which the damper rod restraint is replaced by a circular race, and a heavy fluid such as mercury is used as the damper mass. With the damper mass free to flow in the race, the fluid spreads out uniformly at the end of the damping period, and the symmetry axis of the spinning vehicle exhibits no spin-wobble. Alternatively stated, the fluid acts as an asymmetric damper mass during nutation and as a circularly symmetric mass during spin of the vehicle.

The spreading out of the fluid at small nutation angles is not entirely advantageous, however. When the nutation cone angle is large, the force driving the fluid elements around the race are large, and the fluid "coalesces" into a lump that approximates a point mass (Fig. 9a). As the nutation angle

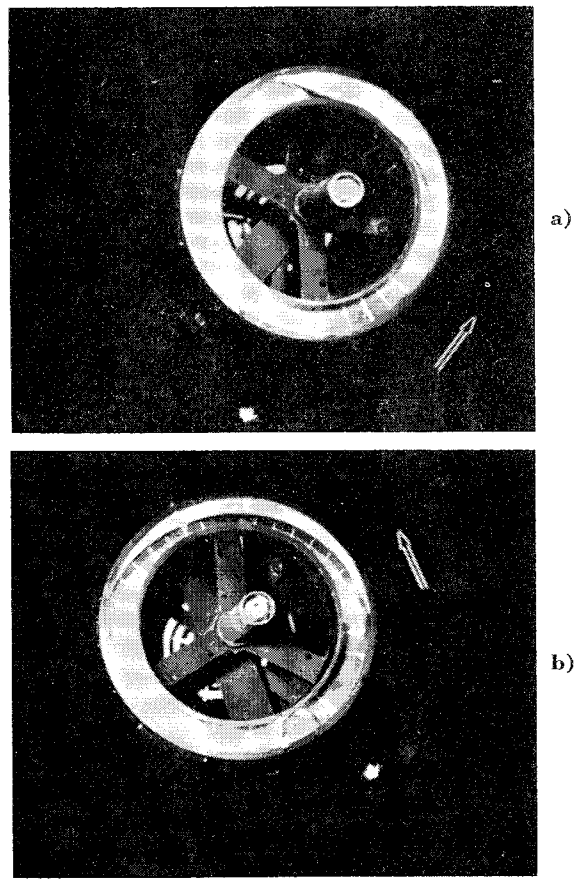

Fig. 9 Typical behavior of a liquid damper mass during nutation decay: a) at beginning of the decay; b) near the conclusion of the decay

decays, these accelerating forces decrease. The centrifugal force field thus gradually "peels off" the side of the lump, and the fluid slowly spreads out or decoalesces as the nutation angle decreases (Fig. 9b). The area of the fluid in contact with the race thus increases, and the friction coefficient is increased effectively. The fluid version of the damper thus should be expected to depart from the fast nutation-synchronous mode earlier than an equivalent mass ball version. Figure 10 shows an experimental comparison of the performance of a ball damper and a fluid damper of the same mass. The viscosity of the fluid was chosen to produce the same damping rate as in the ball mass version during the nutation-synchronous portion of the action. It can be seen that the fluid damper does, indeed, depart from the convex shaped nutation-synchronous damping mode earlier than does the ball version. The small amplitude of the oscillatory behavior in the spin-synchronous regime is typical of fluids.

Thus it appears that, for the same weight, a point mass (ball) damper will exhibit better performance than a fluid circular constraint damper. The spin wobble remaining after the nutation has been damped is the price one pays for this improved performance, but for many applications the size of this wobble is negligible. To an approximation, valid for small wobble angles, the spin wobble half cone angle is given by

$$\gamma_W \simeq [1/(1 - r)](m\rho h/I_P) \qquad (7)$$

For a damper of reasonable mass, this wobble angle is quite small. Hopefully, the additional experimental evidence now being evaluated will provide a better understanding of the relative merits of ball and fluid dampers.

Design Stratagems

The design formulas, Eqs. (4) and (5), indicate the important role played by the frictional coupling between the damper mass and the spinning body. The greater the friction coefficient, the faster does the damper mass extract energy from the nutation and transfer it to spin [Eq. (5)]. With a large frictional force, however, the damper mass is driven out of the nutation-synchronous damping mode at nutation angles that are rather large [Eq. (4)].

It is possible to overcome these conflicting effects in damper performance by two design techniques. The first

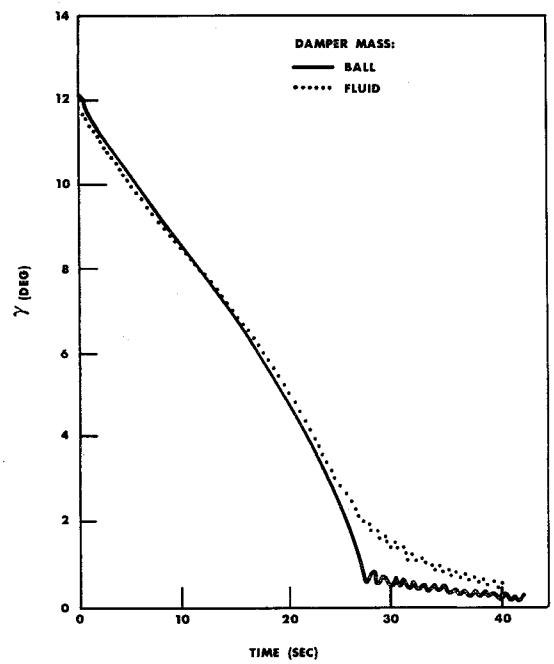

Fig. 10 Comparison of nutation angle decay for a fluid damper mass and a ball damper mass

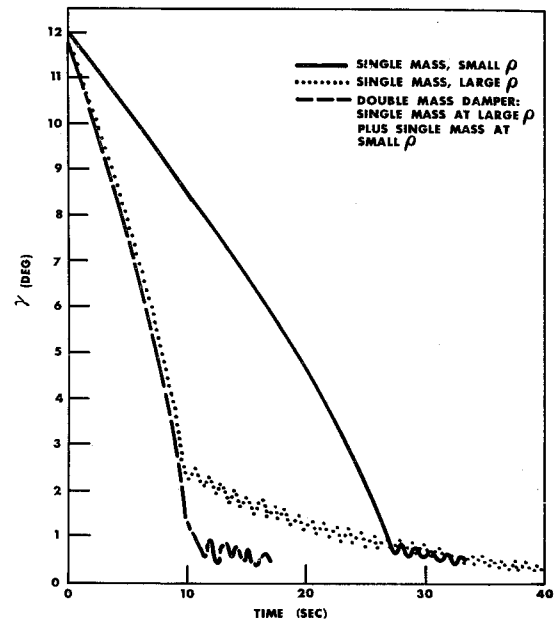

Fig. 11 Performance of a double mass circular constraint damper

is simply to "tailor" the coefficient of friction C_f. By making C_f a very rapidly increasing function of velocity, the damper mass will be strongly coupled to the disk while in the nutation-synchronous mode, thus rapidly transferring energy from nutation to spin. As the frictional force slowly decreases the velocity of the mass relative to the disk, C_f falls, uncoupling the mass just sufficiently to prevent it from "going over the top." Thus a properly tailored C_f will produce a fast nutation-synchronous damping action, while suppressing the onset of the relatively ineffectual spin-synchronous motion. This "tailoring" occurs naturally, to some degree, because of the usually velocity-dependent C_f. Also, it can be accentuated by the use of magnetic clutches, various fluid combinations, and vanes that restrict fluid flow at large γ.

Another technique that decreases the t^*-γ^* conflict is to employ two circular constraint dampers, one of large radius and one of considerably smaller radius. The motion of each damper has been found to be essentially uncoupled from the other. Thus the large radius damper produces fast damping during large nutational motion, whereas the small radius damper continues to damp (albeit more slowly) in the nuta-

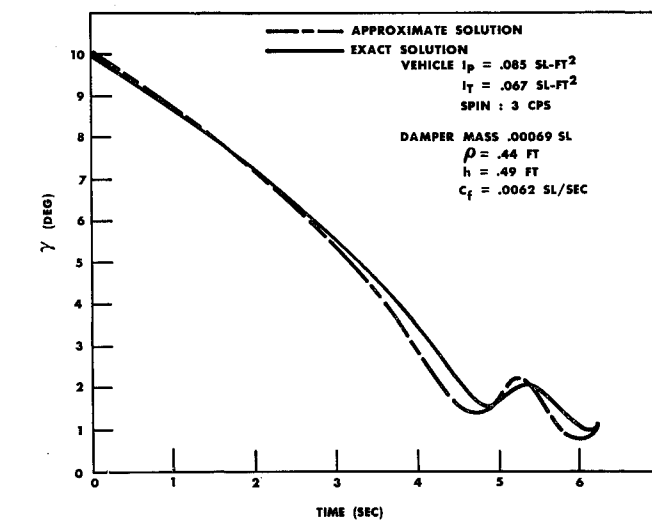

Fig. 12 Comparison of the solutions obtained using the approximate and exact damper equations

tion-synchronous mode after the large damper has ceased its unidirectional motion. Figure 11 illustrates this.

Other techniques, such as combination fluid and ball dampers, suggest themselves as improvements to the basic circular constraint damper design. The particular application of the damper will determine the extent to which such improvements need be employed. In any case, Eqs. (4) and (5)—provided that the inequality (6) is obeyed—can be used in making preliminary damper performance estimates.

Appendix: Approximate Disk-Damper Equations of Motion

The exact equations were approximated by a set of simplified equations that embody only the principal terms. The variables appearing in the equations are defined in Fig. 6.

The angular rate $\dot{\varphi}$ defines the rotation rate of the transverse angular velocity vector $\boldsymbol{\Omega}_t$, that is, the departure of the actual nutation rate of the disk from the nominal rate Ω_{spin}/r. [It is the assumption of $\dot{\varphi} \equiv 0$ and $\varphi = 0$ in the following equations which leads to Eqs. (1) and (2) of the text.] The important lag angle δ is the displacement of the damper mass from its no-friction equilibrium position.

By ignoring the small variation in spin rate which occurs during damping and using only the principal terms of the exact equations, the following rather useful approximate equations are obtained:

$$\dot{\gamma} = -\frac{m\rho h}{I_T}\left(\frac{I_P}{I_T}\right)\Omega_s \sin\delta$$

$$\ddot{\alpha} + \frac{C_f}{m}\dot{\alpha} - \frac{h}{\rho}\left(\frac{I_P}{I_T}\right)^2 \Omega_s{}^2\gamma \sin\delta = -\frac{C_f}{m}\left(\frac{I_P - I_T}{I_T}\right)\Omega_s$$

$$\gamma\dot{\varphi} = -\frac{m\rho h}{I_T}\left(\frac{I_P}{I_T}\right)\Omega_s \cos\delta$$

$$\alpha \equiv \varphi - \delta$$

In Fig. 12 is shown a comparison of the γ vs time solutions using the exact equations and the approximate ones. The agreement that obtains in the fast damping or nutation-synchronous region is typical.

References

[1] Newkirk, H. L., Haseltine, W. R., and Pratt, A. V., "Stability of rotating space vehicles," Proc. Inst. Radio Engrs. **48**, 743–750 (1960).

[2] Haseltine, W. R., "Nutation damping rates for a spinning satellite," Aerospace Eng. **21**, 10–17 (March 1962).

[3] Cartwright, W. F., Trueblood, R. D., and Massingill, E. C., "Circular constraint nutation damper analysis," GM DRL Rept. TM 62-205, General Motors Corp. (December 1961).

JUNE 1963 AIAA JOURNAL VOL. 1, NO. 6

Hexagonal Cell Structures under Post-Buckling Axial Load

R. K. McFarland Jr.*

Jet Propulsion Laboratory, California Institute of Technology, Pasadena, Calif.

A method is presented for determining the approximate crushing stress of hexagonal cell structures subjected to axial loading. The purpose of performing this analysis was to determine an approximate analytical relation that can be used to compute the crushing stress of a given hexagonal cell structure. Of additional importance was the determination of the parameters that control the crushing stress and the sensitivity of the crushing stress to variations in these parameters. Experimental verification that was obtained for the resulting relations indicates that this method of analysis provides very effective upper and lower limits on the mean crushing stress of hexagonal cell structures. The purpose of the analysis was to provide rational means by which hexagonal cell structures can be designed for use as energy absorbers.

Nomenclature

A = basic panel element dimension
B = horizontal projection of basic panel element dimension
B_t = true length of B
D = width of cell wall
F = mean crushing stress
f = mean crushing force
K = P_w/D
M_{yp} = plastic moment per unit of length
P_w = width of basic panel element
q_{yp} = shear yield stress
S = cell minor diameter
t = cell wall thickness
U = energy
β = $(1 + 3\sin^2\theta)^{1/2}$
θ,ϕ = angles representing degree of collapse of a single cell element
ψ = angle representing shear deformation of a single cell element
σ_{yp} = tensile yield stress

Presented at the IAS Annual Summer Meeting, Los Angeles, Calif., June 19–22, 1962; revision received April 2, 1963. This paper presents the results of one phase of research carried out at the Jet Propulsion Laboratory, California Institute of Technology, under Contract No. NAS 7-100, sponsored by NASA.

* Research Engineer, Engineering Research.

I. Introduction

THIS report presents an upper-bound limit analysis of hexagonal cell structures subject to axial loading. The analysis is an approximate one, assuming a rigid-plastic material with equal yield stress in tension and compression and neglecting the effect of superimposed axial stresses on the yield criterion.

A simple mode of collapse for the hexagonal cell structure is assumed, based on experimental observations, and from this the collapse mechanisms are determined. The limit analysis techniques then are applied to the collapse mechanisms, and the energy of deformation is computed. The energy of deformation then is equated to the change in po-